AeroChem TN-161

NASA CR-132715

NO_x DEPOSITED IN THE STRATOSPHERE BY THE SPACE SHUTTLE

By Harold S. Pergament

and

Roger D. Thorpe

Final Summary Report

Phase I

July 1975

Prepared under Contract No. NAS1-13544 by
AEROCHEM RESEARCH LABORATORIES, INC.
Princeton, NJ

for

NATIONAL AERONAUTICS AND SPACE ADMINISTRATION

NASA CR-132715

TITLE PAGE
USE COVER
AND BLOCK OUT

NO_x DEPOSITED IN THE STRATOSPHERE BY THE SPACE SHUTTLE

By Harold S. Pergament

and

Roger D. Thorpe

Prepared under Contract No. NAS1-13544 by
AEROCHEM RESEARCH LABORATORIES, INC.
Princeton, NJ

for

NATIONAL AERONAUTICS AND SPACE ADMINISTRATION

SUMMARY

The results of initial calculations to determine the total amount of NO_x deposited in the stratosphere by the Space Shuttle Solid Rocket Motors (SRM) are presented. Detailed calculations of the flow properties and chemical composition in the exhaust nozzle and plume were performed, accounting for such effects as gas/particle nonequilibrium and nonequilibrium chemistry in the nozzle, plume shocks (including the Mach disc) and nonequilibrium chemistry in the mixing/afterburning region and downstream of the Mach disc.

The nozzle calculations show that, to within a factor of two, about 4.5 lbm/sec of NO_x leaves the two SRM's. The total amount of NO_x deposited in the stratosphere is related to the amount leaving the nozzle via an Overall Plume Enhancement Factor (OPEF), whose value depends upon the influence of afterburning and shocks in enhancing the exit plane NO_x mole fraction. Initial calculations show that the OPEF ≈ 2, indicating the mass flow of NO_x in the plume to be ≈ 10 lbm/sec at 30 km altitude with a possible error factor of $\stackrel{x}{\div} 4$. The error bounds account for possible errors in input data (e.g. reaction rate coefficients), and the neglect of several phenomena (e.g. recirculating flow in the shuttle base region and intersecting plumes from the two SRM's) which may prove to be important.

For a vehicle velocity of 3750 ft/sec, therefore, the NO_x deposition rate in the stratosphere is about 2.7×10^{-3} lbm/ft (4 g/meter), to within a factor of 4.

TABLE OF CONTENTS

LIST OF TABLES

LIST OF TABLES (continued)

LIST OF FIGURES

I. INTRODUCTION

An accurate determination of the total amount of NO_x deposited in the stratosphere by the Space Shuttle Solid Rocket Motors (SRM) requires that detailed exhaust plume $[NO_x]$* distributions be calculated, accounting for the effects of afterburning and plume shocks. These effects will increase the amount of NO_x in the plume over its value at the nozzle exit plane, the amount of the increase being defined as the Overall Plume Enhancement Factor (OPEF). The total amount of NO_x deposited in the stratosphere† is, then, the amount "leaving" the exhaust plume. Figure 1 shows a schematic of the variation of Local Plume Enhancement Factor (LPEF)‡ as a function of distance from the

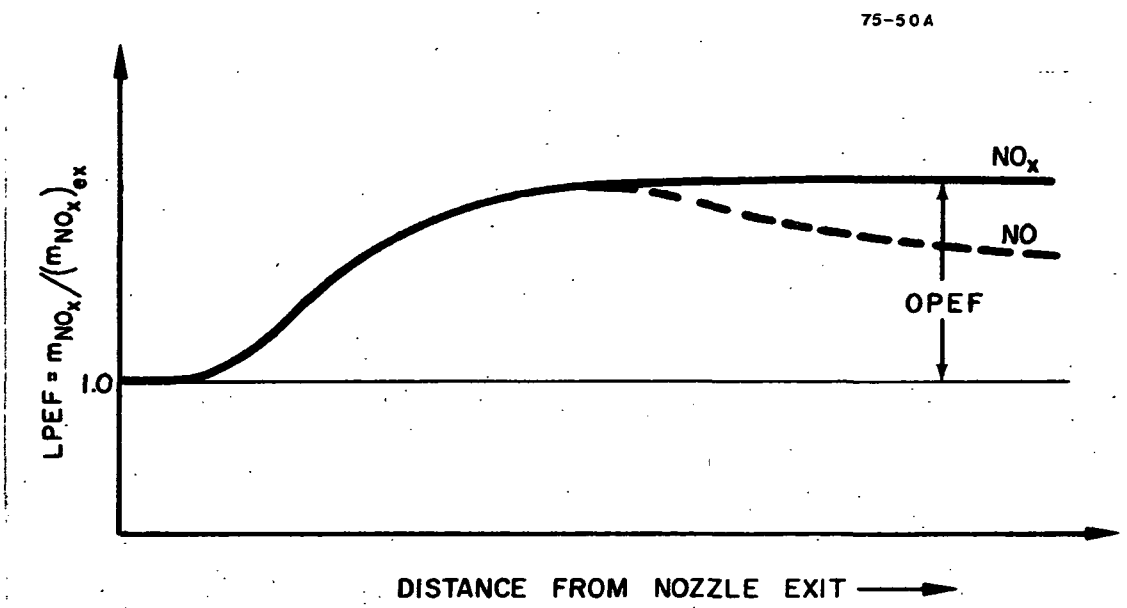

FIG. 1 SCHEMATIC SHOWING DEFINITIONS OF LOCAL PLUME ENHANCEMENT FACTOR (LPEF) AND OVERALL PLUME ENHANCEMENT FACTOR (OPEF)

* $[NO_x]$ is defined as a local concentration of NO_x.

† NO_x consists of NO, NO_2 and N_2O.

‡ The LPEF is defined as the mass flow of NO_x at any axial station ($\dot{m}_{NO_x}$) divided by the mass flow of NO_x leaving the nozzle, $(\dot{m}_{NO_x})_{ex}$. $\dot{m}_{NO_x}$ is calculated from $\dot{m}_{NO_x} \propto \int_{-\infty}^{\infty} \rho u Y_{NO_x} r \, dr$, where ρ, u and Y_{NO_x} are gas density, velocity and mass fraction of NO_x, respectively and r is radial distance from the axis.

nozzle exit. Note that the LPEF increases to an asymptotic value, the OPEF, which defines the end of the "NO_x plume". There are no plume reactions which will decrease local values of $[NO_x]$; plume reactions involving NO_x far from the nozzle exit, in the cooler regions of the flow, convert NO to NO_2.

The procedure followed in the present study has been to obtain initial estimates of $[NO_x]$ at the nozzle exit plane and in the plume via a series of simplified calculations which neglect the effects of (i) two-dimensional flow and gas/particle interactions in the nozzle and (ii) shocks in the plume. These results give both an order of magnitude estimate of $[NO_x]$ in the nozzle and plume and the dependence of the predictions on uncertainties in some of the input data, e.g. reaction rate coefficients and turbulent mixing rates. Next, a more detailed analysis was performed in which the effects noted above were accounted for and the OPEF calculations made. This report presents the principal results of both the simplified and detailed calculations and concludes with a first determination of the total amount of NO_x deposited in the stratosphere by the Space Shuttle Solid Rocket Motors.

II. INITIAL NOZZLE AND PLUME CALCULATIONS

A. Nozzle

The nozzle exit plane $[NO_x]$ was initially determined via one-dimensional kinetic calculations. These calculations were made using nozzle pressure, temperature and velocity distributions calculated via a standard nozzle thermochemical equilibrium code (from AFRPL) as input to an Aero-Chem-developed nonequilibrium streamline code (NEQSLINE).[1] Additional input to the code were the equilibrium composition in the combustion chamber (Table I) and a suitable chemical reaction mechanism and rate coefficients (Table II). The upper and lower bounds of the rate coefficients given in Table II are our best estimates based on the available experimental data. Figure 2 shows that the calculated NO_x mole fraction* freezes near the throat at a level about an order of magnitude greater than that predicted by the equilibrium calculation at the exit. (The 1-D EQUIL. curve was computed by the standard thermochemical equilibrium program.) The "STD. RATES (FULL)" curve was computed via NEQSLINE using all the reactions listed in Table II except Reactions D1-D6. A detailed examination of the reaction rates for individual reactions showed that reactions NO2, NO4, NO5, NO8, NO10, P3,

* In the nozzle NO is the dominant constituent of NO_x; N_2O and NO_2 mole fractions are orders of magnitude less than that of NO.

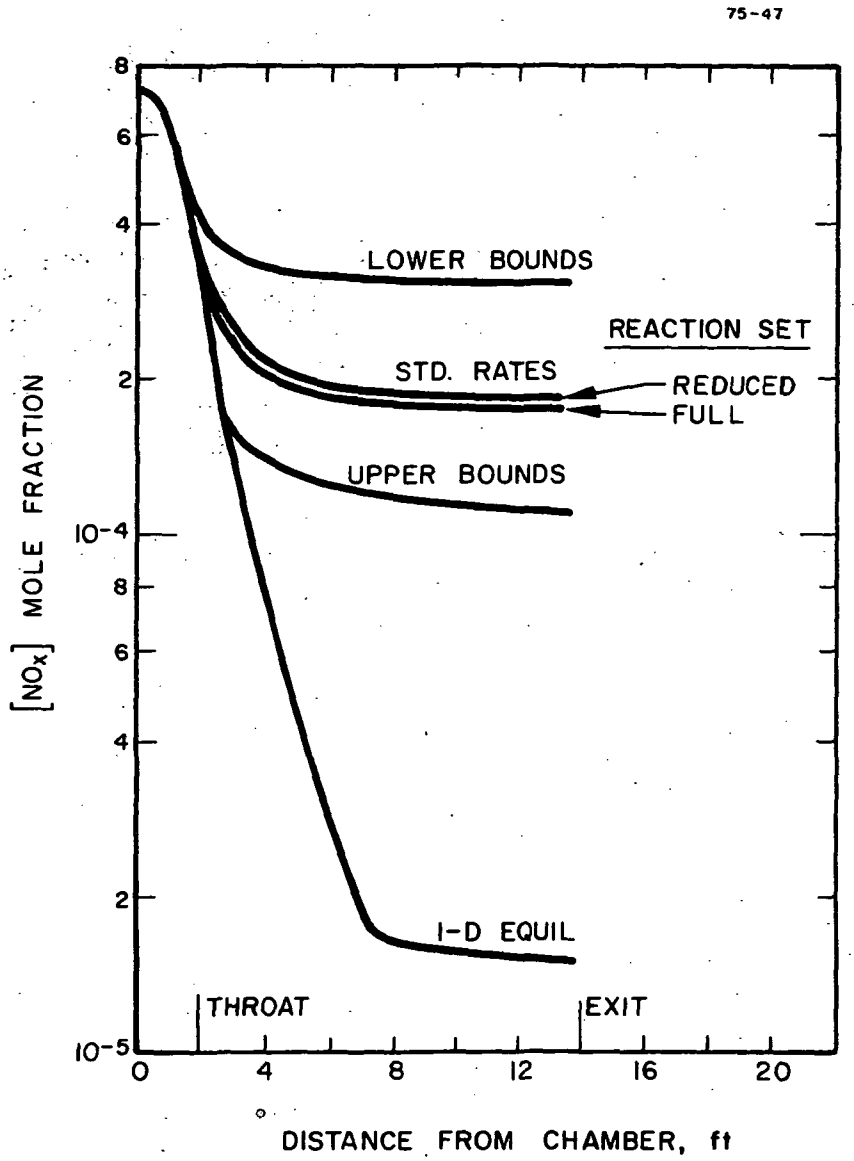

FIG. 2 NO_x MOLE FRACTION IN SPACE SHUTTLE SRM

One-dimensional kinetic calculations assuming gas/particle equilibrium

P5, P6, P10 and P11 could probably be eliminated with little effect on $[NO_x]$. The "STD. RATES (REDUCED)" curve shows that, indeed, eliminating the above reactions does not significantly influence the results. Additional nozzle calculations were made with the remaining NO_x Production/Depletion and NO_x Precursor reactions set to their estimated maximum and minimum rates re-

TABLE I. SPACE SHUTTLE SRM NOZZLE PROPERTIES

Propellant Composition	Wt. %	ΔH_f^0 (kcal/mole)
NH_4ClO_4	69.6	-70.69
Al	16.0	0.0
$C_{6.884}H_{10.089}O_{0.218}N_{0.264}$	12.0	-12.0
$C_{6.15}H_{6.97}O_{1.17}N_{0.03}$	2.0	-28.3
Fe_2O_3	0.4	-197.3

Equilibrium Calculations

	Chamber	Exit Plane
Pressure, atm	41.6	1.08
Temperature, ^oK	3400	2330
A/A*	--	6.7
Mass Fraction Al_2O_3 particles	0.30	0.30

Gas Composition, Mole Fraction

CO	2.49(-1)
CO_2	1.74(-2)
HCl	1.43(-1)
H	3.80(-2)
H_2	2.77(-1)
OH	9.11(-3)
H_2O	1.52(-1)
N_2	9.92(-2)
N	6.19(-6)
NO	7.05(-4)
O	7.45(-4)
O_2	1.62(-4)
Cl	1.30(-2)
HNO	1.15(-6)
N_2O	7.93(-8)
NH	2.78(-6)
NH_2	1.07(-5)

TABLE II. SPACE SHUTTLE SRM NOZZLE/PLUME REACTION MECHANISM

$$k_f = A\, T^{-N} \exp(B/RT)$$

	Heat Release	A[a]	N	B (cal/mole)	Upper[b] Error Bound	Lower[c] Error Bound
HR1	$O + O + M \rightleftarrows O_2 + M$	1.0(-29)	1.0	0	30	30
HR2	$O + H + M \rightleftarrows OH + M$	1.0(-29)	1.0	0	30	30
HR3	$H + H + M \rightleftarrows H_2 + M$	2.8(-30)	1.0	0	30	30
HR4	$H + OH + M \rightleftarrows H_2O + M$	2.0(-28)	1.0	0	10	10
HR5	$CO + O + M \rightleftarrows CO_2 + M$	1.0(-29)	1.0	-2500	3	30
HR6	$OH + OH \rightleftarrows H_2O + O$	1.0(-11)	0	-1000	5	5
HR7	$OH + H_2 \rightleftarrows H_2O + H$	5.0(-11)	0	-5200	3	3
HR8	$O + H_2 \rightleftarrows OH + H$	5.0(-11)	0	-8460	3	3
HR9	$H + O_2 \rightleftarrows OH + O$	3.0(-10)	0	-16500	3	3
HR10	$CO + OH \rightleftarrows CO_2 + H$	5.0(-13)	0	-600	3	3
HR11	$H + Cl + M \rightleftarrows HCl + M$	5.5(-31)	1.0	0	30	30
HR12	$HCl + OH \rightleftarrows H_2O + Cl$	7.2(-12)	0	-3250	30	30
HR13	$H + HCl \rightleftarrows Cl + H_2$	8.8(-11)	0	-4620	10	10
HR14	$OH + Cl \rightleftarrows HCl + O$	3.0(-11)	0	-5000	30	30
	NO Production/Depletion					
NO1	$O + N_2 \rightleftarrows NO + N$	1.3(-10)	0	-76000	3	3
NO2	$N + O_2 \rightleftarrows NO + O$	2.2(-11)	0	-6250	3	3
NO3	$NO + H \rightleftarrows N + OH$	1.5(-10)	0	-47000	5	5
NO4	$N + CO_2 \rightleftarrows NO + CO$	3.0(-13)	0	-34000	30	10
NO5	$NO + NO \rightleftarrows N_2O + O$	2.1(-12)	0	-64000	5	5
NO6	$NO + H_2 \rightleftarrows HNO + H$	1.0(-11)	0	-54600	10	30
NO7	$HNO + Cl \rightleftarrows HCl + NO$	3.0(-11)	0	-1600	10	100
NO8	$NH + NO \rightleftarrows N_2O + H$	1.0(-12)	0	-4200	100	100
NO9	$NO + H + M \rightleftarrows HNO + M$	5.5(-29)	1.0	600	3	10
NO10	$NO + M \rightleftarrows O + N + M$	8.3(-29)	1.0	-149000	30	30

[a] cm-molecule-sec units

[b] multiply A by upper error bound to get maximum possible value of rate coefficient

[c] divide A by lower error bound to get minimum possible value of rate coefficient

(continued)

TABLE II

(continued)

	NO Precursor		A[a]	N	B (cal/mole)	Upper[b] Error Bound	Lower[c] Error Bound
P1	$N_2O + H$	$\rightleftarrows N_2 + OH$	1.3(-10)	0	-15200	3	10
P2	$N_2O + H_2$	$\rightleftarrows H_2O + N_2$	1.0(-13)	0	0	100	100
P3	$N_2O + CO$	$\rightleftarrows N_2 + CO_2$	3.3(-13)	0	-17400	10	10
P4	$N_2O + M$	$\rightleftarrows N_2 + O + M$	6.7(-11)	0	0	30	30
P5	$NH + Cl$	$\rightleftarrows HCl + N$	2.0(-11)	0	-4200	10	100
P6	$NH + H$	$\rightleftarrows H_2 + N$	1.0(-11)	0	-4200	30	100
P7	$NH + OH$	$\rightleftarrows H_2O + N$	2.3(-10)	0	-2000	3	3
P8	$NH_2 + Cl$	$\rightleftarrows NH + HCl$	1.0(-10)	0	0	3	100
P9	$NH_2 + H$	$\rightleftarrows NH + H_2$	5.0(-11)	0	0	3	100
P10	$NH + H + M$	$\rightleftarrows NH_2 + M$	3.0(-30)	1.0	0	100	10
P11	$N + N + M$	$\rightleftarrows N_2 + M$	5.6(-30)	1.0	0	10	10
	NO/NO_2						
D1	$NO_2 + NO_2$	$\rightleftarrows NO+NO+O_2$	4.0(-12)	0	-27000	3	3
D2	$NO + O + M$	$\rightleftarrows NO_2 + M$	3.0(-33)	0	2000	3	3
D3	$NO_2 + O$	$\rightleftarrows NO + O_2$	1.7(-11)	0	-600	3	3
D4	$NO_2 + H$	$\rightleftarrows NO + OH$	5.8(-10)	0	-1480	3	3
D5	$NO + CO_2$	$\rightleftarrows NO_2 + CO$	3.3(-12)	0	-81600	30	30
D6	$NO + O$	$\rightleftarrows NO_2 + h\nu$	6.6(-12)	2.0	0	3	3

spectively. These results, also shown in Fig. 2, serve to give a preliminary estimate of the probable error bounds on the calculated $[NO_x]$ at the nozzle exit plane.

B. Afterburning Plume

In order to get a 'feeling' for the potential increase of $[NO_x]$ in the plume due to afterburning, a series of calculations were made with the Aero-Chem parallel mixing/chemistry (LAPP) code[2] using an expanded plume boundary* as the dividing streamline. Initial conditions for the afterburning calculations (given in Table III) were obtained by assuming a chemically frozen

* The expanded plume boundary is defined here as the radius of the inviscid boundary (dividing streamline) at which ambient pressure is reached.

TABLE III. INPUT DATA FOR SPACE SHUTTLE SRM PLUME AFTERBURNING CALCULATIONS[a] ALONG EXPANDED PLUME BOUNDARY AT 30 km

	Initial Conditions	Free Stream Conditions
Radius, ft	47.1[b]	
Velocity, ft/sec	1.04(4)[c]	3.52(3)
Temperature, ^{o}K	1130.	229.
Pressure, atm	0.0118	0.0118
Composition, Mole Fraction		
CO	2.33(-1)	
CO_2	2.09(-2)	
HCl	1.54(-1)	
H	5.47(-3)	
H_2	2.79(-1)	
OH	4.57(-4)	
H_2O	1.41(-1)	
N_2	8.41(-2)	7.90(-1)
N	1.44(-8)	
NO	1.44(-5)	
NO_2	5.35(-12)	
O	6.20(-6)	
O_2	1.32(-6)	2.10(-1)
Cl	2.16(-3)	
Al_2O_3	7.99(-2)	

[a] Using the LAPP code[2]

[b] Actual expanded radius is 33.4 ft. The radius used for these calculations is an 'equivalent' radius that accounts for the mass flow from both SRM nozzles.

[c] $A(B) = A \times 10^{B}$.

one-dimensional expansion from the nozzle exit plane to the ambient pressure at 30 km, and solving simultaneously the continuity, momentum and energy equations. The initial 'equivalent' radius used in the plume calculations is $\sqrt{2}$ larger than the calculated radius to account for the total mass flow from the two SRM's.

The reaction mechanism used in the afterburning calculations includes the HR1-HR14, NO1, NO2, NO3, P11 and D1-D6 reactions of Table II. Typical results are shown in Fig. 3, which plots the ratio of the local $[NO_x]$ to the frozen $[NO_x]$ (i.e. if afterburning were neglected) throughout the plume.† This demon-

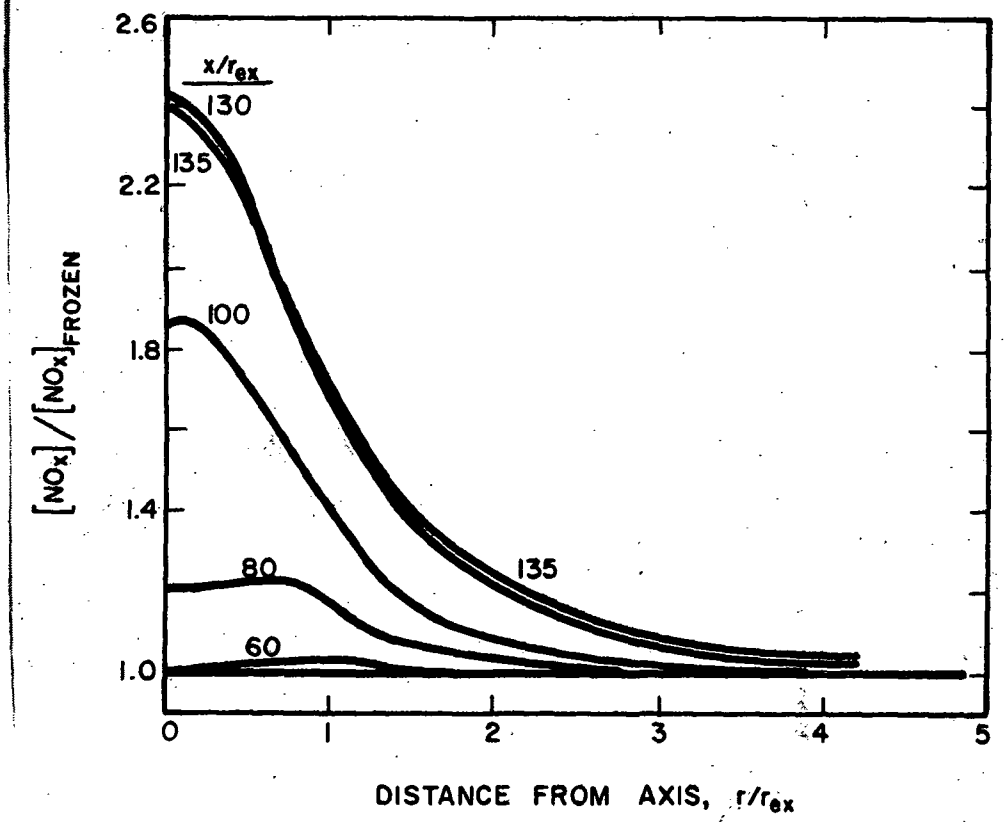

FIG. 3 INFLUENCE OF AFTERBURNING ON PLUME NO_x CONCENTRATIONS
Space shuttle SRM; 30 km altitude; r_{ex} = 47.1 ft; initial temperature = 1130°K

† Note that the Local Plume Enhancement Factor (LPEF) is related to the area under the curve at each axial station. (See definition on p. 1)

strates the direct effect of afterburning in enhancing plume [NO_x] concentrations, the maximum increase being a factor of about 2.4. If we arbitrarily increase the initial temperature from 1130°K (used to obtain the results in Fig. 3) to 2000°K (to account for gross uncertainties in this simplified analysis)* the maximum increase in NO_x over its frozen value is a factor of about 35! This result indicates the importance of accurately establishing the initial temperature in this type of "expanded plume boundary" calculation. Additional parametric calculations were made to determine the effects, on [NO_x], of uncertainties in rate coefficients for reactions governing the direct production of [NO_x] and those controlling the radical concentrations. These results will be presented in the final report.

C. Mach Disc

The potential influence of the Mach disc on [NO_x] in the plume was determined by using the NEQSLINE code, starting just downstream of the Mach disc with post-shock properties (assuming frozen chemistry through the shock) as initial conditions. The Mach disc location was estimated from the empirical correlation of Lewis and Carlson,[3] modified for free-stream velocity effects by D'Attore and Harshbarger.[4] For the purpose of this calculation the pressure distribution between the Mach disc and second plume shock was assumed to be similar to the pressure distribution from the nozzle exit to the throat. The temperature was then determined from a constant γ calculation.

Figure 4 shows the results of the Mach disc calculation using both the standard set of rate coefficients (Table II), and a reaction mechanism in which the NO and P reaction rates (Table II) are set to their upper and lower bounds. About an order of magnitude increase in [NO_x] is seen to occur as the flow passes through the Mach disc (using the standard rates), due primarily to the high temperatures ($\approx$ 3000°K) in this region. For reference, the chamber value of [NO_x] is also shown. This result indicates that the Mach disc will make an important contribution to local plume [NO_x] levels.

III. OVERALL PLUME ENHANCEMENT FACTOR CALCULATIONS

The calculations discussed in Section II were directed at determining local effects and trends important in determining approximate levels of [NO_x] in the nozzle and plume. Calculations aimed at more accurately determining the total amount of NO_x in the plume are discussed below.

* Temperature was varied since [NO_x] is strongly dependent on local plume temperatures.

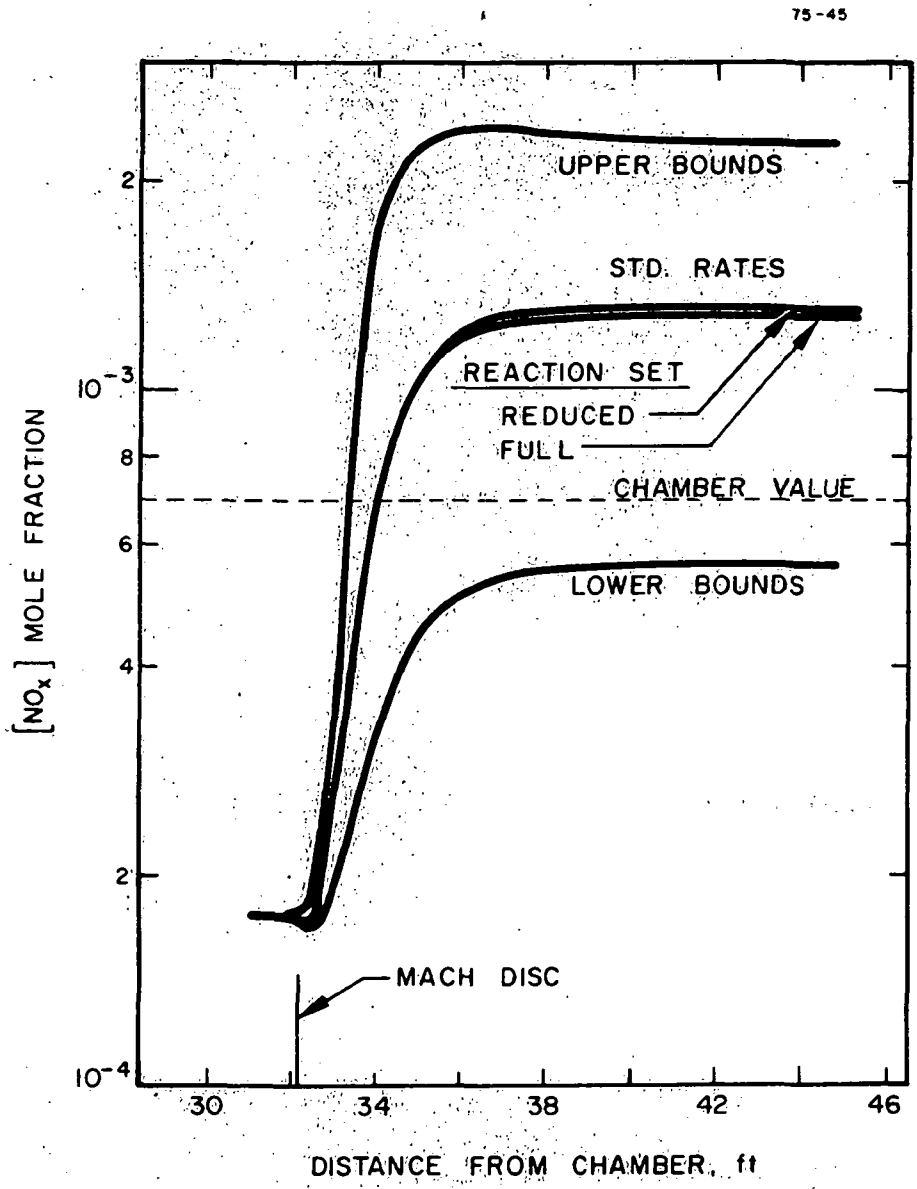

FIG. 4 NO_x MOLE FRACTIONS ALONG AXIS DOWNSTREAM OF MACH DISC

One-dimensional kinetic calculations assuming gas/particle equilibrium

A. Nozzle

The AeroChem fully-coupled nozzle program (FULLNOZ)[5] was used to calculate gas and particle properties in the Space Shuttle nozzle and to assess the effects of gas/particle nonequilibrium on $[NO_x]$. This calculation utilized the actual nozzle contour as input (in contrast to the one-dimensional calculations discussed in Section II.A). The calculated pressure and temperature

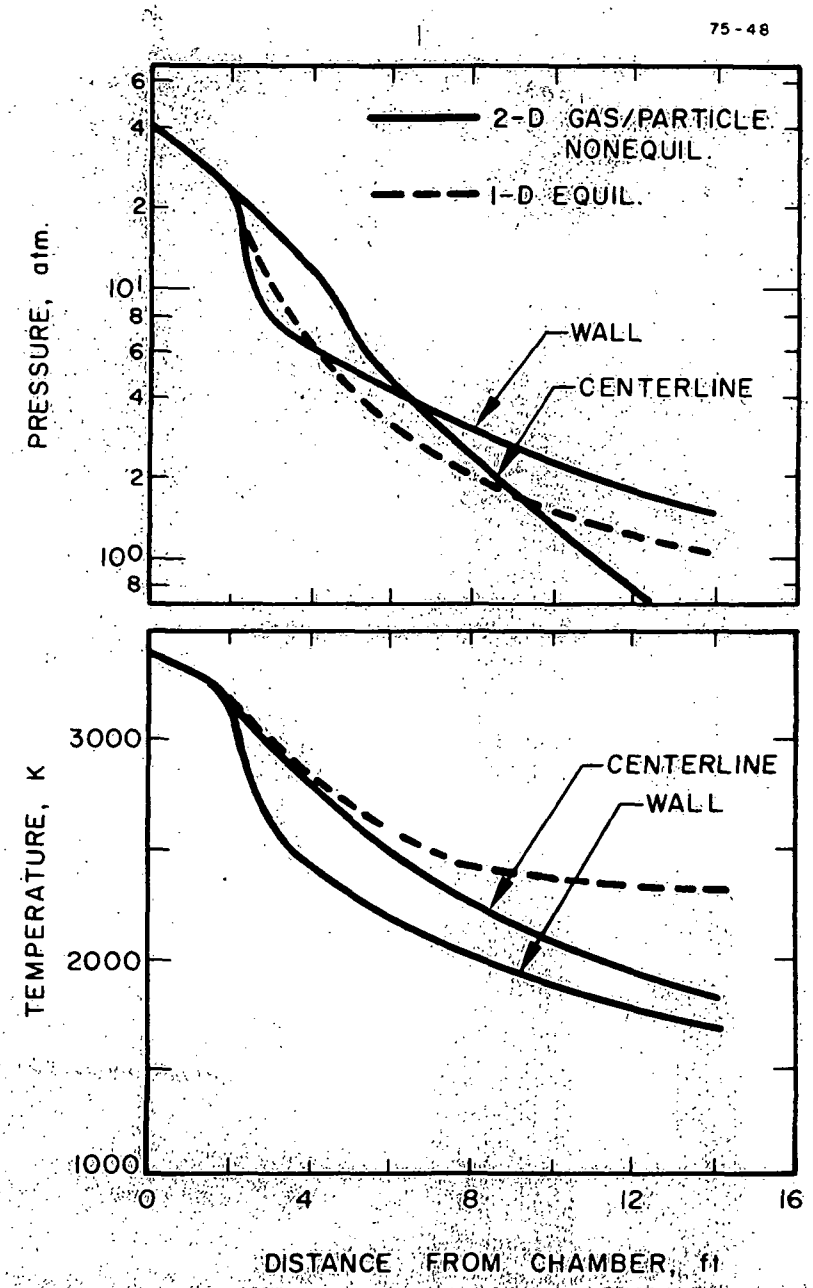

FIG. 5 PRESSURE AND TEMPERATURE DISTRIBUTIONS IN SPACE SHUTTLE SRM

distributions along the wall and centerline are given in Fig. 5, together with the one-dimensional equilibrium results. These results are typical of bell-shaped nozzles, i.e. the flow near the wall rapidly expands just downstream of the throat, giving lower wall pressures in this region. The exit plane wall pressure however is higher than the centerline pressure, i.e. $p_{\text{¢}} = 7.2$ psia and $p_{wall} = 21$ psia. The gas temperature distributions do not follow the pressure distributions because of the influence of solid particles. In fact, the

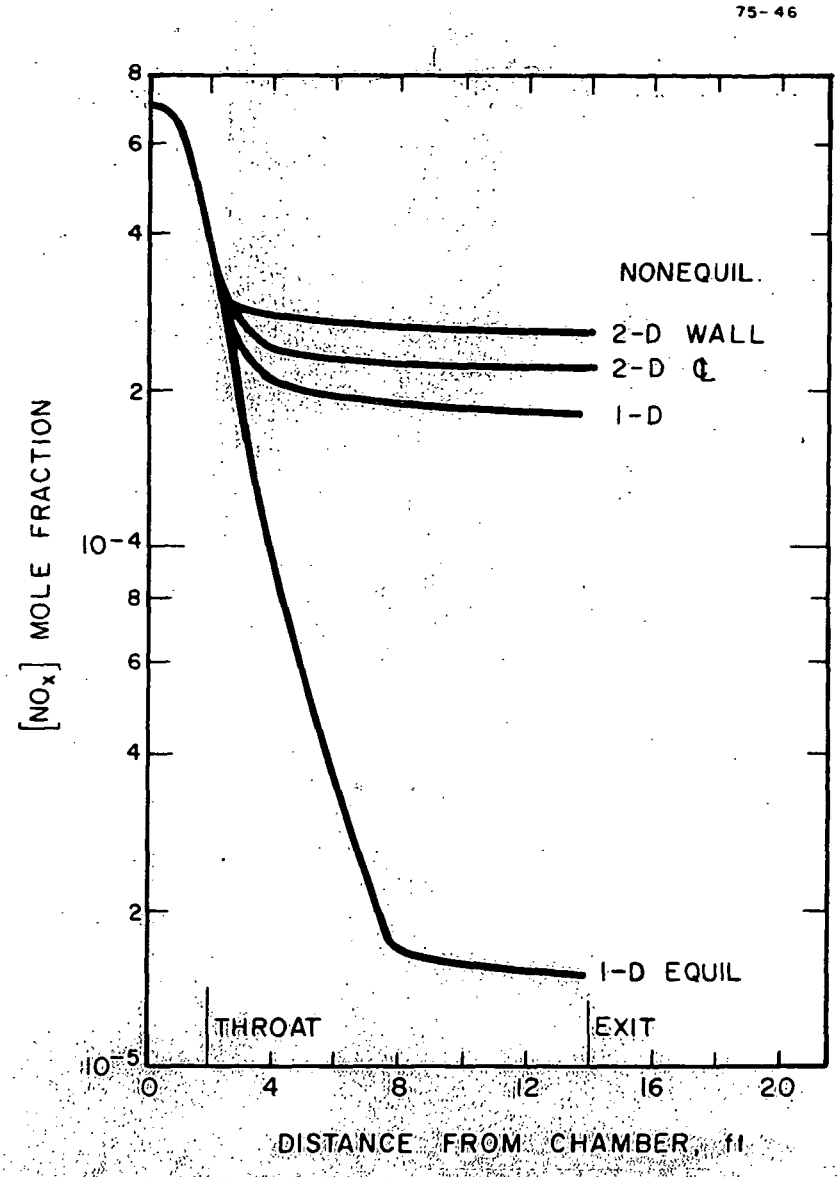

FIG. 6 NO_x MOLE FRACTION IN SPACE SHUTTLE SRM
A comparison between 1-D equilibrium, 1-D kinetic and 2-D kinetic calculations

coupling between the gas and particle flows results in the exit plane gas temperature reaching a maximum value (of 2170°K) off-axis at $r/r_{ex} \approx 0.85$.

Figure 6 compares calculated values of NO_x mole fractions along the centerline and wall, (2-D kinetic) with those computed by the 1-D kinetic and 1-D equilibrium programs. The difference between the 1-D kinetic and 2-D kinetic values at the exit plane is within the anticipated error bounds of $[NO_x]$.

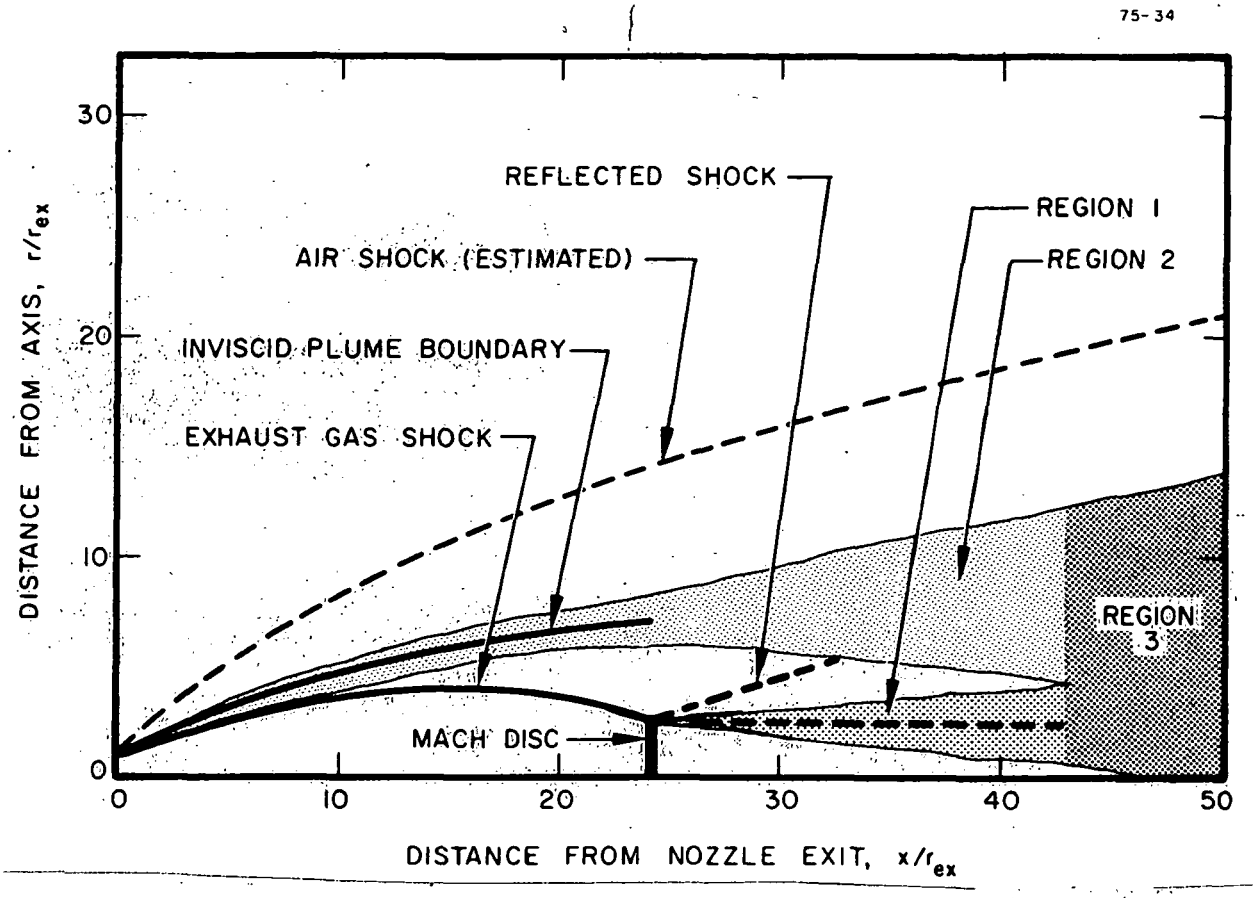

FIG. 7 SPACE SHUTTLE SHOCK STRUCTURE AND MIXING REGIONS

B. Plume

The procedure used to determine the enhancement of NO_x in the plume due to afterburning and shocks was to (1) locate the plume shocks via the AeroChem underexpanded rocket plume code (the AIPP code)[6] and (2) compute the NO_x production using the LAPP code.[2] The shock structure shown in Fig. 7 was scaled from a previous AIPP calculation of a Minuteman (MM) Stage 1 plume in a similar flow region. The LAPP code was then applied to three regions of importance: (1) an inner mixing zone (Region 1) in which the high temperature and pressure exhaust gas that has passed through the Mach disc mixes with lower temperature exhaust products that have passed through the reflected shock; (2) an outer mixing zone (Region 2) where cool exhaust products which have passed through the exhaust gas shock mix with air that has passed through the air shock; and (3) the merged shear layer (Region 3) which is initiated where (1) and (2) meet. Region 1 is characterized by an axial decay in pressure from the post-shock value to ambient. Regions 2 and 3 are treated as constant pressure mixing zones.

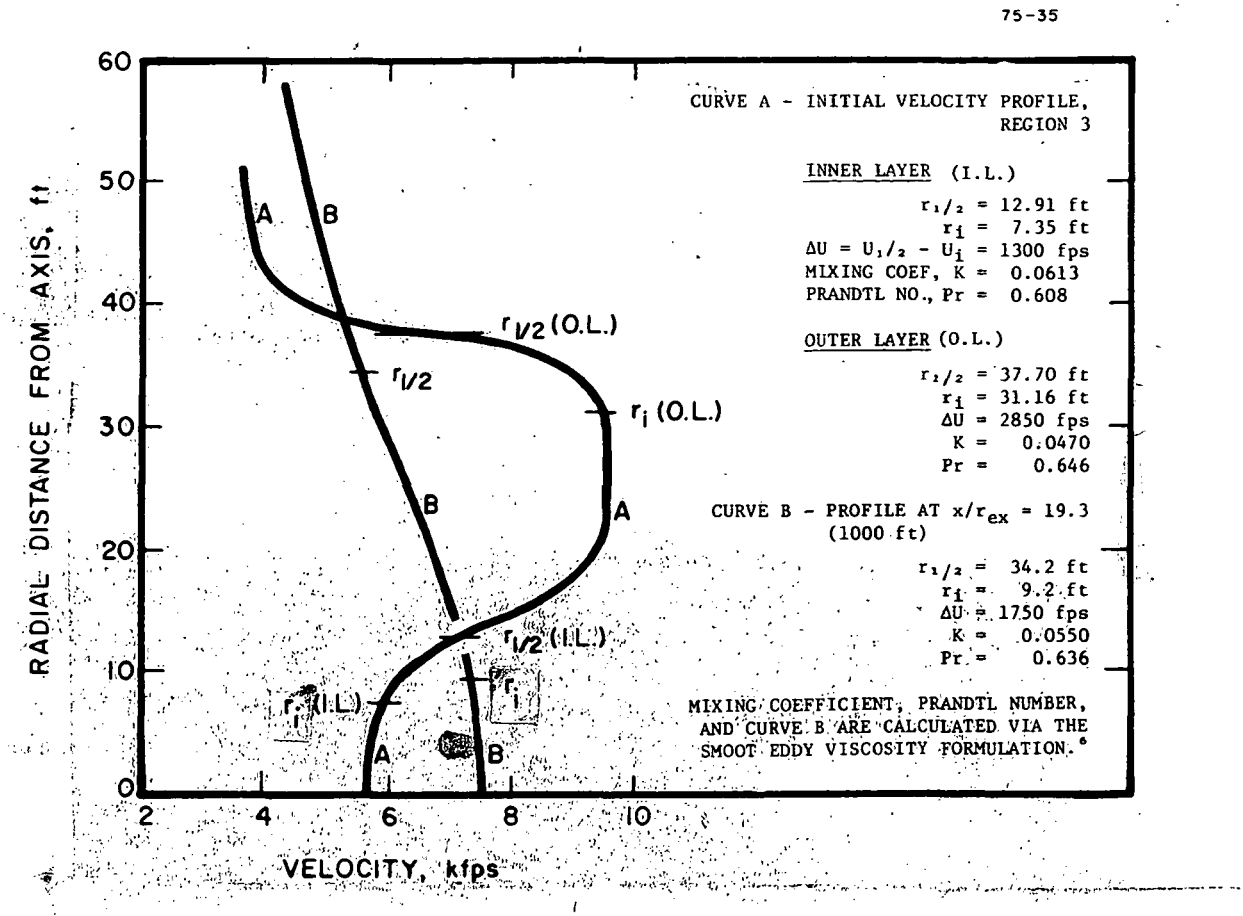

FIG. 8 MERGED SHEAR LAYER LENGTH AND VELOCITY SCALES FOR USE WITH LAPP CODE

1. Calculation Procedure

The calculations for Regions 1 and 2 utilized the standard version of the LAPP code. Region 3, however, is initially characterized by two distinctly different shear layers. The turbulent mixing within this region cannot therefore be adequately described by the single eddy viscosity normally provided for in the code. Consequently, the program was modified to calculate separate characteristic length and velocity scales for the two shear layers until the position of the velocity maximum reaches the centerline. (See Fig. 8.) At this point the program proceeds with the viscosity computation in the normal manner. In addition, the empirical formulation for eddy viscosity developed by Stowell and Smoot,[7] obtained by correlating data for reacting and non-reacting jets into moving secondary streams, has been added to the code. Parametric runs have been made using both the Donaldson/Gray[8] and Smoot[7] eddy viscosity formulations. The reaction mechanism employed was the HR1-14, NO1-3, P11 set given in Table II. Thus far, NO → NO_2 reactions have not been considered here, but will be treated in subsequent calculations.

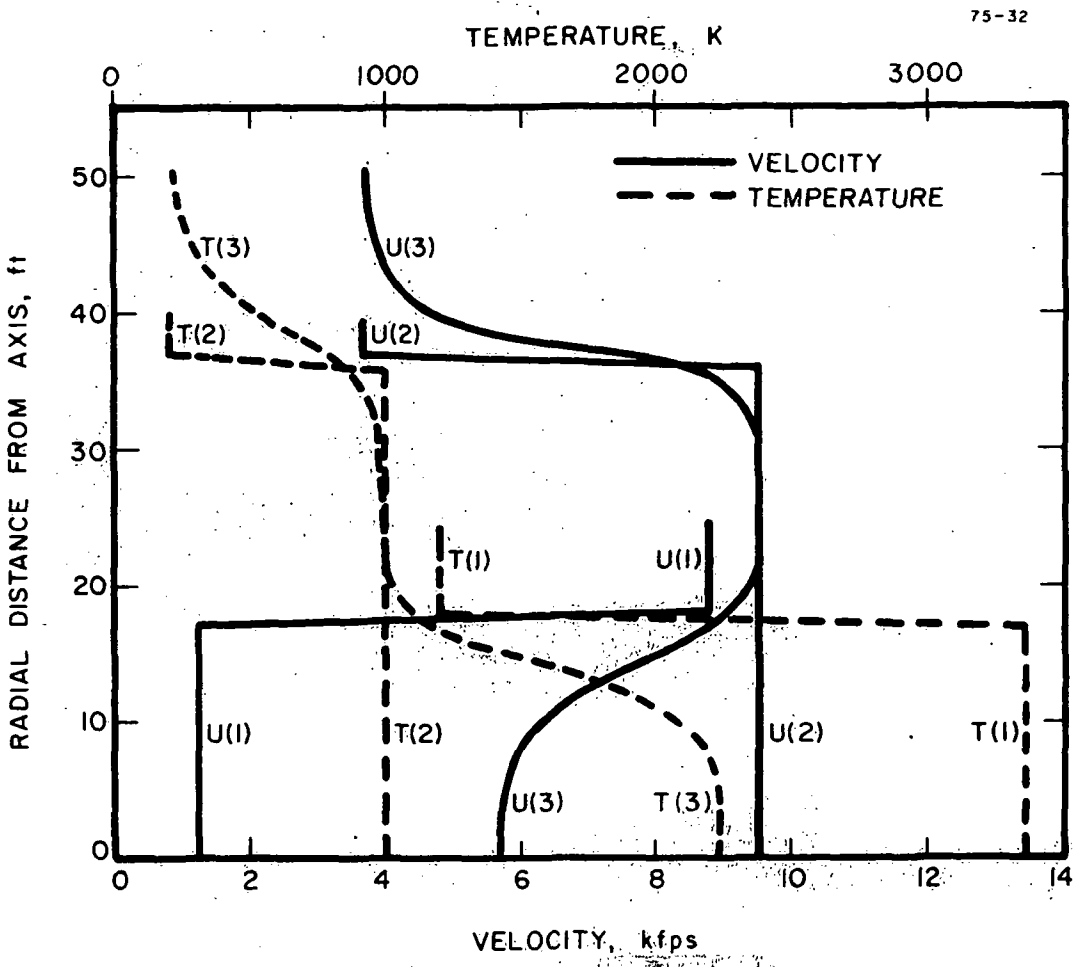

FIG. 9 INITIAL TEMPERATURE AND VELOCITY PROFILES FOR REGIONS 1, 2 AND 3

Input data for the three regions are shown in Table IV. The input mole fractions for the Region 1 calculations were obtained by extending the non-equilibrium nozzle calculations, using NEQSLINE, to the location of the Mach disc. The input for Region 2 was scaled from the MM stage 1 AIPP calculation. The Region 1 calculation extended from the Mach disc to ambient pressure. The extent of Region 2 was identical to that of Region 1. The resulting profiles of temperature, velocity, and composition were then used as input to the Region 3 merged shear layer calculation. The velocity and temperature profiles used as input data for the LAPP calculations are shown in Fig. 9.

2. NO_x Production Downstream of Mach Disc

The total mass flow of NO_x at any axial station was determined by radial integration of the local values from the axis to the edge of the plume. The LPEF was determined by comparing the local value of $[NO_x]$ with that of an

TABLE IV. INITIAL CONDITIONS FOR REGIONS 1, 2, AND 3 CALCULATIONS

	Region 1		Region 2		Region 3	
	Center-line	Free-stream	Center-line	Free-stream	Center-line	Free-stream
Jet Radius, ft	17		36		52	
Vel., ft/sec	1250	8800	9500	3750	5755	3750
Temp., K	3370	1200	1000	220	2233	220
Press., atm	0.0608[a]		0.0118		0.0118	
Mole Fraction						
CO	2.26(-1)	1.76(-1)	1.76(-1)		2.11(-1)	
CO_2	2.50(-2)	3.55(-2)	3.55(-2)		2.12(-2)	
HCl	1.42(-1)	1.27(-1)	1.27(-1)		9.97(-2)	
H	7.32(-3)	1.59(-3)	1.59(-3)		1.11(-1)	
H_2	2.76(-1)	2.24(-1)	2.24(-1)		2.25(-1)	
OH	6.53(-8)	2.54(-6)	2.54(-6)		8.72(-3)	
H_2O	1.45(-1)	1.74(-1)	1.74(-1)		1.23(-1)	
N_2	9.38(-2)	2.60(-1)	2.60(-1)	7.9(-1)	8.70(-2)	7.9(-1)
N	2.58(-9)	1.0(-10)	1.0(-10)		2.05(-6)	
NO	1.61(-4)	1.00(-5)	1.00(-5)		3.01(-4)	
INERT	1.61(-4)	1.00(-5)	1.00(-5)		1.48(-4)	
O	1.73(-8)	1.97(-8)	1.97(-8)		3.02(-3)	
O_2	5.93(-7)	1.49(-7)	1.49(-7)	2.1(-1)	6.96(-4)	2.1(-1)
Cl	5.45(-3)	1.76(-3)	1.76(-3)		3.59(-2)	
Al_2O_3	7.97(-2)	0.	0.		7.36(-2)	

[a] Refers to initial pressure, flow is assumed to expand in region 1 to ambient pressure

inert species having the same molecular weight and initial mass fraction profile. As mentioned previously, the overall plume enhancement factor, OPEF, is the value of the LPEF at the 'end' of the NO_x plume; i.e., the point where the chemical production of NO_x is negligibly small.

The calculation to determine the initial effect of the Mach disc (Region 1) on the LPEF was made using the D/G viscosity model. Because of the uncertainty of applicability of viscosity models in the merged shear layer, parametric runs using both D/G and Smoot models were made to test for their effect on afterburning, and hence, NO_x production in Region 3.

The OPEF results, shown in Table V, indicate that the mass flow of NO_x leaving the plume is 50-65% greater than that leaving the nozzle. Figure 10 shows the axial distribution of the LPEF. It is apparent that most of the NO_x production in the plume occurs immediately behind the Mach disc; little NO_x production occurs in the afterburning region. Indeed, the amount of

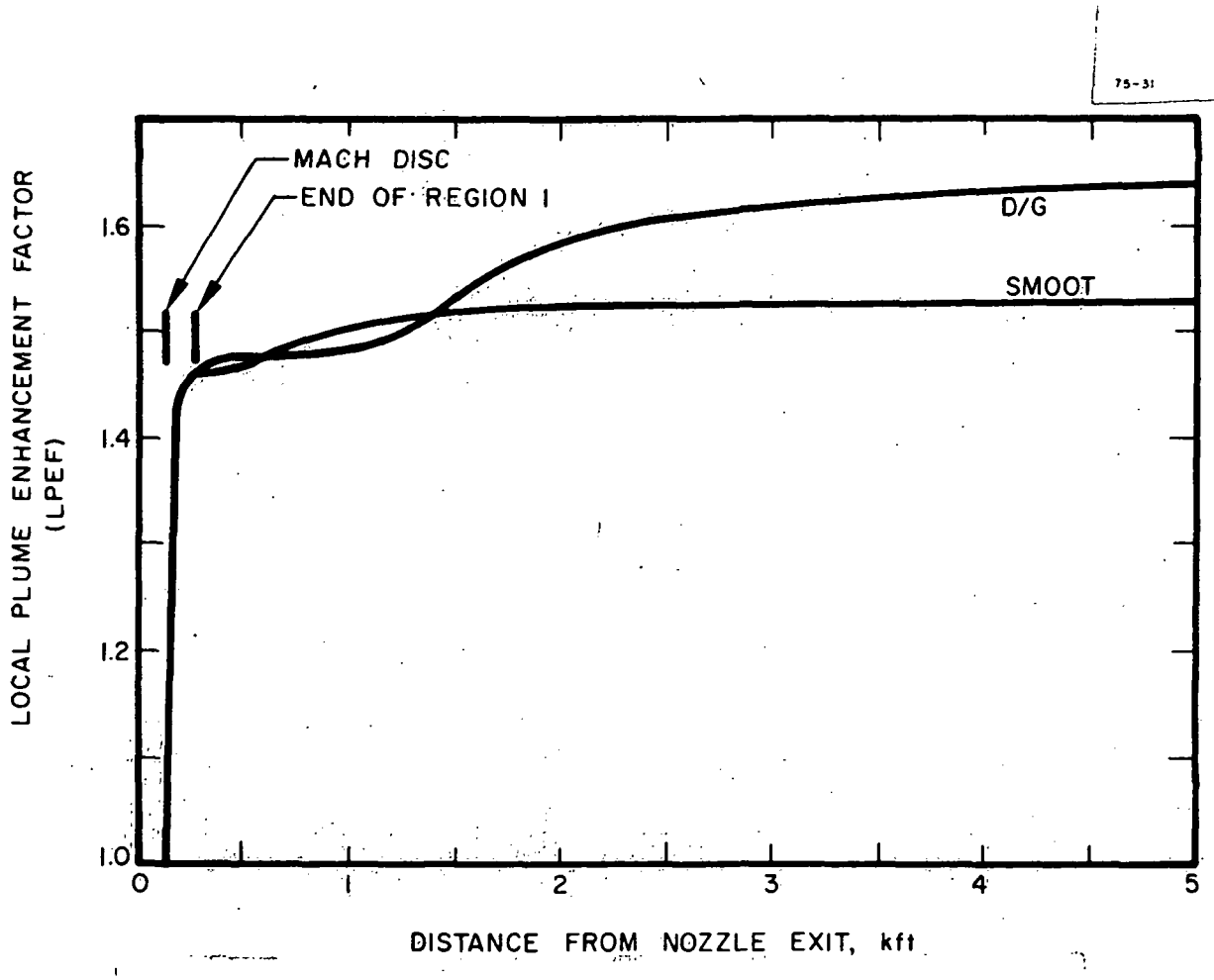

FIG. 10 LOCAL PLUME ENHANCEMENT FACTOR FOR NO_x

TABLE V. OVERALL PLUME ENHANCEMENT OF NO_x AT $x/r_{ex} = 115$

Viscosity Model[a]	OPEF
Donaldson/Gray[8] (K = 0.0248)	1.659
Donaldson/Gray (K = 0.0996)	1.632
Smoot[9]	1.528

[a] K = constant in eddy viscosity expression

afterburning is minimal as seen in the centerline temperature profile of Fig. 11. While it had previously been calculated that locally high concentrations of NO_x could occur due to high plume temperatures (Fig. 4), Fig. 11 shows that the high temperature behind the Mach disc is not maintained. The dissociative effects of the extreme nonequilibrium in this area tend to reduce the temperature quickly, thus inhibiting the formation of large amounts of NO_x. Also, the mixing rate has small effect on the OPEF. While the Smoot model mixes faster than the D/G model, the small amount of afterburning that does occur provides too low a temperature to cause marked NO_x production.

IV. TOTAL NO_x DEPOSITION IN THE STRATOSPHERE

The maximum mass flow of NO_x in the plume is the mass flow leaving the the nozzle multiplied by the OPEF. The total mass flow leaving the two SRM nozzles is about 17,500 lbm/sec. With a mole fraction of NO_x at the nozzle exit of 1.8(-4) ($\stackrel{\times}{\div}$ 2), the mass flow of NO_x at the exit is 4.5 lbm/sec ($\stackrel{\times}{\div}$ 2). The OPEF variation due to eddy viscosity models is relatively small (1.5-1.65). An additional factor of 2 variation is possible however because of uncertainties in calculating the Mach disc size, and because such factors as: (1) recirculating flow in the missile base region; (2) multiple Mach discs; (3) intersecting plumes were neglected in the present calculations.

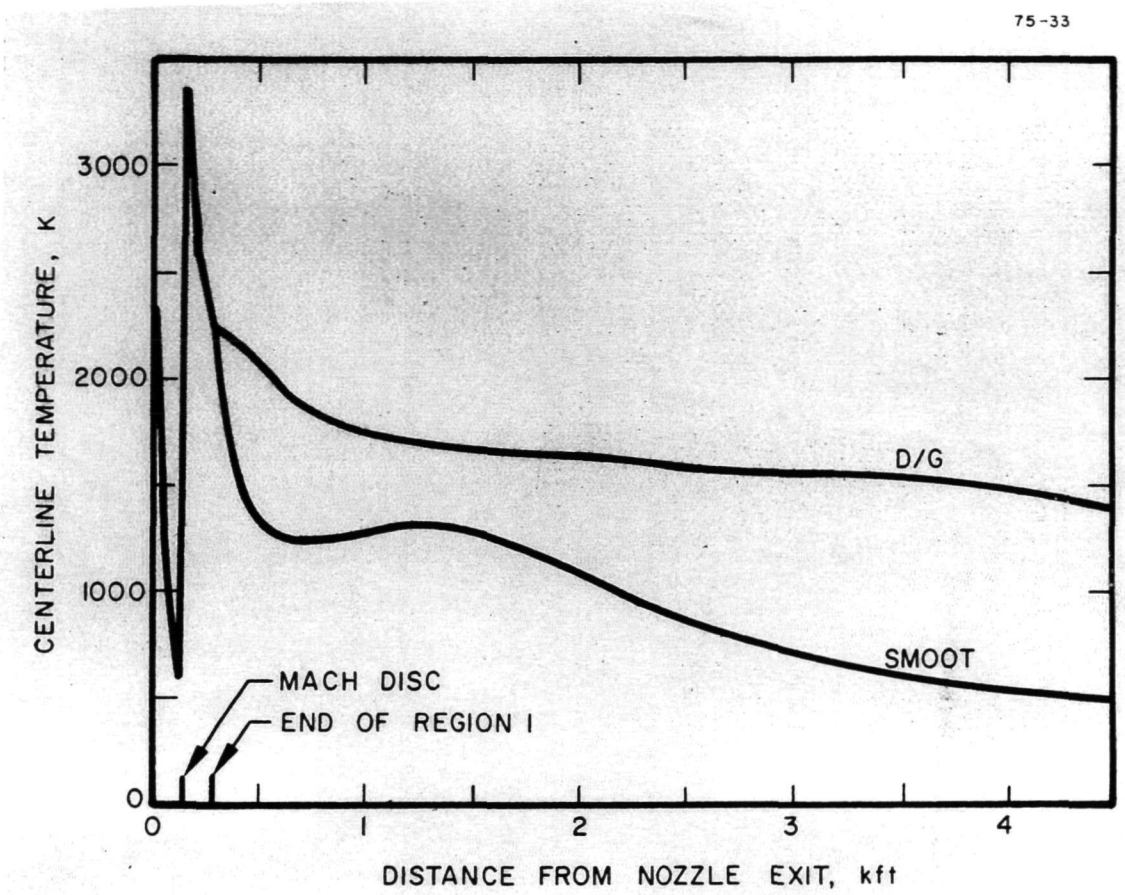

FIG. 11 INFLUENCE OF EDDY VISCOSITY MODEL ON PLUME CENTERLINE TEMPERATURES

Our best estimate thus far for the NO_x mass flow in the plume at 30 km altitude is 10 lbm/sec with a possible error of $\overset{\times}{\div}$ 4. For a vehicle velocity of 3750 fps the NO_x deposition is then 2.7 (-3) lbm/ft (4 g/meter) ($\overset{\times}{\div}$ 4). Our future efforts will be aimed at reducing the error limits on this result by examining the effects of the above uncertainties (see Section V).

V. PLANS

In Phase II of the present study we plan to investigate several phenomenon that have been neglected in the calculations made to date, but which could significantly effect the predicted amounts of NO_x deposited in the stratosphere. This work has been divided into the following three tasks:

A. Interaction of Exhaust Plume with Flow Around Shuttle Body and in the Base Recirculation Region

The plume calculations performed thus far have assumed that (a) the "free stream" Mach number is uniform and equal to the vehicle Mach number and (b) the shuttle base recirculation region is negligibly small. In this task we plan to utilize existing shuttle flow field calculations at stratospheric altitudes to determine actual flow properties approaching the base region. These properties will be input to an analysis of the base recirculation region (e.g. Ref. 9) which will be used to determine inter alia the position of the recompression shock and the composition of the recirculating base region flow entering the air/rocket exhaust mixing region. Of prime concern here is the possibility that, because of the presence of a significantly large base recirculation region, the combustibles in the rocket exhaust products (H_2 and CO) will ignite in the base region and "feed" small quantities of free radicals (H, OH) into the mixing region, thus considerably speeding up the chain-branching steps in the H_2/O_2 reaction mechanism. The overall effect is that plume afterburning would be initiated near the nozzle exit (i.e. the base would act as a flameholder*) rather than far downstream where it would normally occur due to mixing between the exhaust products and ambient air at stratospheric altitudes. The result would be that relatively large quantities of NO_x could be produced in the plume much nearer the nozzle exit plane than was predicted in Section III. The base recirculation region properties will be input to the AIPP code and a calculation performed to determine the total plume NO_x production, including afterburning and shocks. This type of calculation should give a reasonably accurate quantitative assessment of the effect of the shuttle body/base recirculation region on $[NO_x]$ levels in the plume.

B. Intersecting Plumes

As the shuttle altitude increases, the two solid propellant plumes become greatly underexpanded and, in the stratosphere, they will intersect close to the nozzle exit. The present plume calculations have been made by replacing the two intersecting plumes by a single "equivalent" plume having nozzle exit plane properties identical to those of a single nozzle, but with the exit radius increased by $\sqrt{2}$ to give the same total mass flow.† While this assumption is quite reason-

* This "flameholding" effect has been observed in Apollo (first stage) flights.[10] Apollo first stage (F-1 engine), however, is a liquid rocket using a LOX/RP-1 system.

† At lower altitudes, e.g. about 10 km, it is probably more reasonable to treat each plume separately.

able in analyzing the far field mixing/afterburning plume properties, it does not accurately handle the near field shock structure, particularly the shock caused by the intersection of the two plumes. In this task we plan to investigate this near field shock structure and estimate its influence on the OPEF.

C. Shocks Downstream of the First Mach Disc

State-of-the-art plume models generally neglect the existence of the second (and subsequent) Mach discs.* These shocks are known to be present (e.g. from plume shadowgraphs and pressure measurements) but they are always weaker than the first Mach disc. However there is the possibility that appreciable NO_x can be produced behind these downstream shocks. In order to evaluate the significance of this effect we will estimate the shock locations from existing photographic evidence, empirical correlations and pressure rises downstream of the first Mach disc as predicted by the AIPP code. This procedure will give us sufficient information to compute the post-shock gasdynamic properties, which in turn will be input to the NEQSLINE code to determine NO_x production in the post-shock regions. These local NO_x concentrations will be compared with the levels achieved within the second shock cell to assess the importance of downstream shocks.

* Some models do treat two or more shock diamonds, which are formed for rockets with ratios of nozzle exit to ambient pressure less than about three.

VI. REFERENCES

1. Pergament, H.S. and Mikatarian, R.R., "Prediction of Minuteman Exhaust Plume Electrical Properties," AeroChem TP-281, June 1973.

2. Mikatarian, R.R., Kau, C.J., and Pergament, H.S., "A Fast Computer Program for Nonequilibrium Rocket Plume Predictions," AeroChem TP-282, Final Report, AFRPL-TR-72-74, NTIS AD 751 984, August 1972.

3. Lewis, C.H., Jr. and Carlson, D.J., "Normal Shock Location in Underexpanded Gas and Gas-Particle Jets," AIAA J. 2, 776-777 (1964).

4. D'Attore, L. and Harshbarger, F.C., "Parameters Affecting the Normal Shock Location in Underexpanded Gas Jets," AIAA J. 3, 530-531 (1965).

5. Pergament, H.S. and Thorpe, R.D., "A Computer Code for Fully-Coupled Rocket Nozzle Flow," AeroChem TP-322, July 1975.

6. Pergament, H.S. and Kelly, J.T., "A Fully-Coupled Underexpanded Rocket Plume Program (The AIPP Code). Part I. Analytical and Numerical Techniques." AeroChem TP-302a, Final Report, AFRPL-TR-74-59, November 1974.

7. Stowell, D.E. and Smoot, L.D., "Turbulent Mixing Correlations in Free and Confined Jets," AIAA/SAE 9th Propulsion Conference, 5-7 November 1973, AIAA Paper 73-1194.

8. Donaldson, C. duP., and Gray, K.E., "Theoretical and Experimental Investigations of the Compressible Free Mixing of Two Dissimilar Gases," AIAA J. 4, 2017-2025 (1966).

9. Smoot, L.D., Simonson, J.M. and Williams, G.A., "Development and Evaluation of an Improved Aft-Plume Model," Naval Weapons Center TP-5521, November 1973.

10. Draper, J.S., "The Role of the Plume Separated Region as a Flameholder on the Apollo Vehicle," AIAA Paper 75-243, 1975.